

# High-Field, $\mu\text{J}$ -Class THz Pulses from a Laser Wakefield Accelerator

N. H. Matlis<sup>\*</sup>, G. R. Plateau<sup>\*,†</sup>, J. van Tilborg<sup>\*</sup>, C. G. R. Geddes<sup>\*</sup>,  
Cs. Tóth<sup>\*</sup>, C. B. Schroeder<sup>\*</sup>, E. Esarey<sup>\*,\*\*</sup> and W. P. Leemans<sup>\*,\*\*</sup>

<sup>\*</sup>Lawrence Berkeley National Laboratory, Berkeley, CA 94720, USA

<sup>†</sup>École Polytechnique, Palaiseau 91128, France

<sup>\*\*</sup>University of Nevada, Reno, Nevada 89557, USA

**Abstract.** We present observation and characterization of microjoule-MV/cm-level THz pulses from a laser wakefield accelerator. THz emitted as coherent transition radiation from the plasma-vacuum boundary is collected and refocused by off-axis parabolas to a test stand where a suite of diagnostics is performed, including energy measurement by a Golay cell and electro-optic sampling of the spatio-temporal electric field using a probe pulse split from the main laser. Frequency Domain Holography is also implemented for the first time to capture spatio-temporal field distributions in a single shot. The four techniques strongly corroborate detection of THz pulses of  $\sim 0.4$  ps duration, with peak fields of several hundred kV/cm and energies of 5 – 10  $\mu\text{J}$ . The advantages and disadvantages of each technique are discussed.

**Keywords:** Terahertz, CTR, Wakefield, Diagnostics, Electro-optic sampling, Holography.

**PACS:** 41.60.Dk, 41.75.Jv, 42.30.Rx, 42.40.Kw, 52.38.-r, 52.38.Kd, 52.59.Ye, 52.25.Os

## INTRODUCTION

Terahertz radiation produced by laser wakefield accelerators (LWFAs) has received increasing attention as both a source and as a diagnostic of the performance of the accelerator. Because electron bunches produced by LWFAs are very short (10's of fs), they can radiate coherently in the 1 – 10 THz range when transitioning across a sharp dielectric boundary [1,2]. The resultant “T-ray” pulses can have high fields ( $\sim$  MV/cm) and high energies (10's of  $\mu\text{J}$ ) in sub-ps pulse durations, making them attractive for both probing and pumping of samples. In addition, their inherent synchronization with the laser system allows for multiple-pulse, multi-color experiments. Because the properties of the THz pulses are directly related to those of the electron bunches producing them, they are also well-suited for use as a diagnostic tool to measure electron bunch parameters.

In this paper, four distinct techniques are used to characterize the THz pulses: pulse energy integration using a Golay cell; two variations on spatially-resolved electro-optic (EO) sampling, one with sensitivity to the sign of the THz field, and one without; and Frequency Domain Holography (FDH), a single-shot interferometric measurement applied for the first time to measure the spatio-temporal field profile of THz pulses. While each technique has advantages and disadvantages, and each yields different details about the THz pulses, quantitative data on field strengths and pulse energies

can be compared, yielding cross-checks and benchmarks. Quantitative comparison of the results as well as discussion of the THz pulse properties show that the THz pulses had energies of several  $\mu\text{J}$  and fields of several hundred  $\text{kV}/\text{cm}$ .

## DETECTION TECHNIQUES

A 10 TW laser pulse (45 fs, 800 nm) was focused onto the leading edge of a supersonic gas jet of Helium. A wakefield, produced behind the laser pulse in the ionized Helium, traps and accelerates electrons to energies of  $\sim 10 - 80$  MeV. The electron bunches that are produced are sub-50 fs in duration [3,4]. When the accelerated electrons exit the plasma (gas jet), they emit coherent transition radiation (CTR) at the plasma-vacuum boundary in the THz regime. The CTR is emitted in a forward-directed cone, with a cone angle that is dependent on the energy of the electrons. An off-axis parabola ( $f/2$ ) with a 3" diameter, placed at an angle of 19 degrees with respect to the laser axis, is used to collect and collimate a portion of the THz radiation. The collected radiation is then transported to a test stand and refocused with a second off-axis parabola ( $f/2.33$ ). A poly-ethylene window is used to couple the THz out of the vacuum-chamber.

### Pulse Energy Integration with a Golay Cell

Initial characterization of the THz pulses was done with a Golay cell, which is a compact acousto-optic device that responds to THz pulses in the 0.02 – 20 THz range with a voltage spike proportional to the integrated energy of the pulse. A calibration of  $0.59 \mu\text{J}/\text{V}$  [5] coupled with an observed saturation level of 1.44 V corresponds to a full-scale detection limit of  $E_{\text{sat}} \approx 0.85 \mu\text{J}$ . Because the THz pulses generated by the LWFA accelerated electron bunches had energies that significantly exceeded this saturation level, it was necessary to implement a controlled method of attenuation. Two approaches were used to limit the energy incident on the Golay cell (Fig. 1).

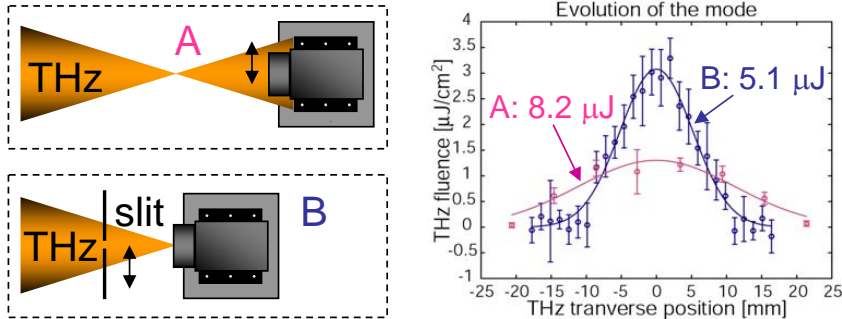


**FIGURE 1.** A Golay cell collects THz radiation exiting the chamber. In the first experiment, the Golay cell is translated (A), in the second, a pair of metal plates forming a slit is translated (B). In the first technique, the Golay cell was moved downstream of the THz focus until the aperture of the cell was considerably smaller than the expanding THz beam. By scanning the cell transversely to the beam, the horizontal beam profile was measured, and assuming cylindrical symmetry of the THz, a pulse energy of  $8.2 \mu\text{J}$  was inferred

from integration of the profile. However, in the event that there is significant asymmetry in the beam, this method could under or over estimate the pulse energy. In the second technique, the Golay cell was placed at the THz focus while a slit was inserted into the beam upstream of focus, strongly aperturing the beam in one dimension. The slit was then scanned allowing reconstruction of the vertically-integrated upstream beam profile. Since the entire beam was sampled, an integration of the profile results in an unambiguous measurement of the pulse energy, found to be 5.1  $\mu\text{J}$ . In both measurements, the THz mode profile was found to be well characterized by a Gaussian.

## 2D Electro-Optic Sampling: Non Sign-Resolved

Although Golay cell measurements quickly provide energy information about the THz pulses, a more sophisticated method, such as EO sampling, is required to characterize the energy distribution and intensity at the focus. In EO sampling, THz radiation acts like a static electric field inducing a second order birefringence proportional to the local, instantaneous field strength. An ultrashort diagnostic laser pulse, timed to coincide with the THz, experiences a polarization rotation which is translated to an amplitude modulation by use of a polarizer (termed “analyzer”). The probe pulse duration is much shorter than the THz optical period, and the transmitted probe is imaged onto a CCD, capturing a spatial cross-section of the THz pulse to be measured. In the “non sign-resolved” configuration, the analyzer is set to minimize the probe transmission in the absence of THz field, making it very sensitive to low field strengths. The relative transmission of the probe through the analyzer is given by [6]

$$\frac{I_T}{I_0} = \sin^2 \frac{\Gamma_{THz}}{2}, \quad \text{where } \Gamma_{THz} = 2\pi \frac{L}{\lambda_0} \eta_0^3 r_{41} E_{THz} \quad (1)$$

is the birefringent phase retardation,  $L$  is the crystal thickness,  $\eta_0$  is the index of refraction of GaP at the probe wavelength of  $\lambda_0 = 800 \text{ nm}$ ,  $r_{41}$  ( $\sim 0.95 \times 10^{-12}$ ) [7] is the second order nonlinear coefficient, and  $E_{THz}$  is the field of the THz pulse.

With a polarizer placed upstream of the interaction, extinction ratios of  $\sim 1 \times 10^{-3} - 1 \times 10^{-4}$  (limited by residual depolarization from imperfections in the EO crystal) were achieved, allowing THz fields above  $\sim 3 \text{ kV/cm}$  to be detected. For polarization rotations greater than  $90^\circ$ , interpretation of the probe transmission becomes ambiguous, resulting in an upper limit to the measureable field strength for this technique of about  $260 \text{ kV/cm}$  (for a  $200 \mu\text{m}$  thick GaP crystal).

A disadvantage of this scheme is that while positive and negative THz fields produce polarization rotations of opposite direction, both directions result in the same change in transmission, making it impossible to resolve the sign of the field. However, the lack of sign-discernment coupled with the high sensitivity makes this technique ideal for characterizing the distribution of energy in space and time within the THz pulse. By scanning the probe pulse delay, a sequence of images was acquired, which were first summed to produce a time-integrated mode profile, and then spatially integrated to produce a temporal profile (Fig. 2). Integration of both space and time then gives the total energy contained in the THz pulse, which was

found to be  $E_{\text{pulse}} \sim 5.8 \mu\text{J}$ , consistent with the Golay cell results. Peak electric fields of  $E_{\text{peak}} \sim 200 \text{ kV/cm}$  were measured.

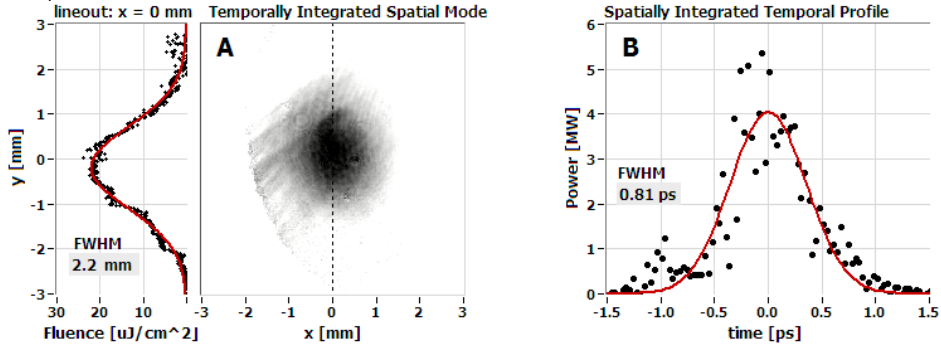


FIGURE 2. Temporally integrated spatial profile (A) and spatially integrated temporal profile (B) of the THz pulse.

## 2D Electro-Optic Sampling: Sign-Resolved

The advantage of high sensitivity in the above technique comes at the expense of ability to resolve the sign of the field, motivating implementation of another technique (sign-resolved EO sampling) for cases where the mapping the electric field oscillations (complete with sign and phase information) is desirable. In sign-resolved EO sampling, a quarter-wave plate (QWP) is inserted before the analyzer providing a base level of polarization rotation which is added to that induced by the THz. Since positive and negative THz fields rotate the probe polarizations in opposite direction, the rotations will either add or cancel, causing the transmission through the analyzer to either increase or decrease compared to the zero-field case. The transmission in this case is now given by [6]:

$$\frac{I_T}{I_0} = \frac{1}{2} \left( 1 - \cos \Gamma_{\text{THz}} \cos^2 2\delta + \sin \Gamma_{\text{THz}} \sin 2\delta \right), \quad (2)$$

where  $\delta$  is the angle of the QWP with respect to the crystal z-axis. The presence of a background transmission ( $I_T = \frac{1}{2} I_0$ ) in this technique necessarily results in a reduction in the sensitivity ( $E_{\text{min}} \sim 10 - 50 \text{ kV/cm}$ ).

A scan of the probe delay reveals additional details of the THz spatio-temporal field structure not observable in the non-sign-resolved experiment. Notably, at delays near the peak of the pulse, there is a negative field feature of only  $\sim 0.3 \text{ mm}$  diameter, while at delays farther from the peak there are positive and negative ring structures of increasing size up to  $\sim 3 \text{ mm}$  diameter (Fig. 3). The sequence of sign-resolved images was used to reconstruct a 2D space-time cross-section of the THz pulse field (Fig. 4). The asymmetrical illumination of the ring structure is manifested as a tilt in the energy front of the pulse with a slope of  $\sim 5 \cdot c$  (where  $c$  is the speed of light). The presence of coupling between spatial features of the mode and its temporal evolution may be an indication of an imaging aberration in the transport line, which is known to cause spatio-temporal coupling. Alternatively, the vertical asymmetry of the collection geometry combined with chromatic dispersion [2] and vertical asymmetry in the

emitting structure (gas jet) may also produce spatio-temporal features. A lineout of the cross-section shows a near-single-cycle behavior of the temporal field profile at the center of the mode, with a field strength of  $E_{\max} \sim 200$  kV/cm, and an intensity envelope of  $\Delta t_{\text{FWHM}} \sim 0.36$  ps.

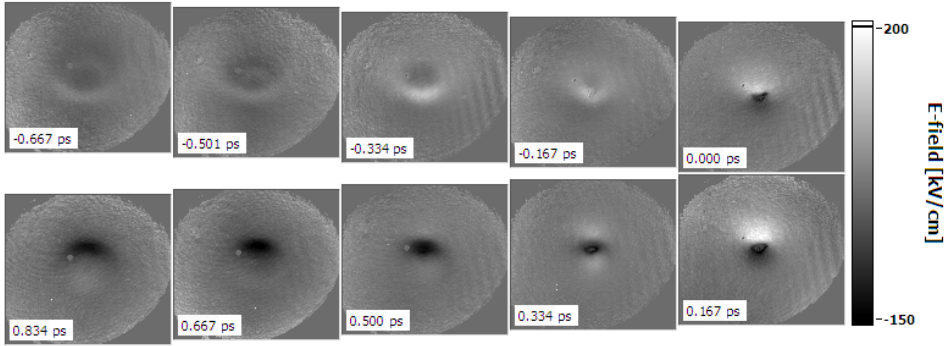


**FIGURE 3.** Evolution of the spatial profile of the THz field vs delay. Time in ps.

Closer inspection of spatial modes near the peak of the THz pulse reveals a feature which can be attributed to the pulse-field exceeding the upper limit of the measurement technique: a local peak in the middle of the negative trough. For negative fields greater than a theoretical value of about -260 kV/cm, the phase retardation is greater than  $\pi/2$ , causing the transmission to increase anomalously as shown in Fig. 4.

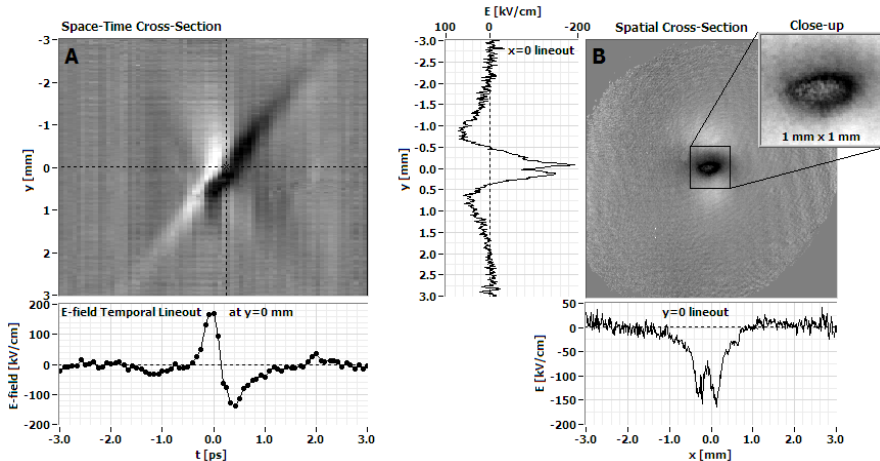


**FIGURE 4.** Space-time cross-section (A) of the field of the THz pulses reconstructed from a delay scan using 2D sign-resolved EO sampling. Spatial cross-section (B) showing inversion (closeup). The observed inversion occurs at a field strength near -200 kV/cm, in reasonable agreement with the theoretical value, providing a good benchmark for the field strength measurement. Accounting for this anomalous behavior, corrected fields of  $\sim 300$  kV/cm were reached in these experiments.

## Frequency Domain Holography

While the sign-resolved EO sampling technique is capable of producing space-time cross-sections of the THz pulse fields, the need to scan delay makes it time-consuming and susceptible to shot-to-shot fluctuations. Real-time optimization and characterization of the THz pulses therefore calls for a single-shot technique. Frequency Domain Holography (FDH) [8,9], an interferometric technique which records temporal phase-shift profiles in a single shot, was implemented to address this need. In this method, two collinear but temporally separated chirped laser probe pulses are combined with the THz in the GaP crystal. The polarization is aligned with a principal axis of the induced birefringence in which case the EO effect imparts a phase-shift of  $\Phi_{\text{THz}} = \frac{1}{2} \Gamma_{\text{THz}}$  without rotating the polarization.

The pulses are sent into a spectrometer and an FFT based algorithm is applied to recover the THz field profile. The interaction point is imaged to the spectrometer slit, producing space-time cross-sections on every shot. Measurements using FDH confirm a pulse duration on the order of  $\sim 1$ ps, and a field strength of  $E_{\text{max}} \sim 400$  kV/cm (Fig. 5). The tilt of the energy front observed in the sign-resolved EO sampling data is also reproduced, however preliminary analysis has not yet recovered the expected sensitivity to the sign of the field.

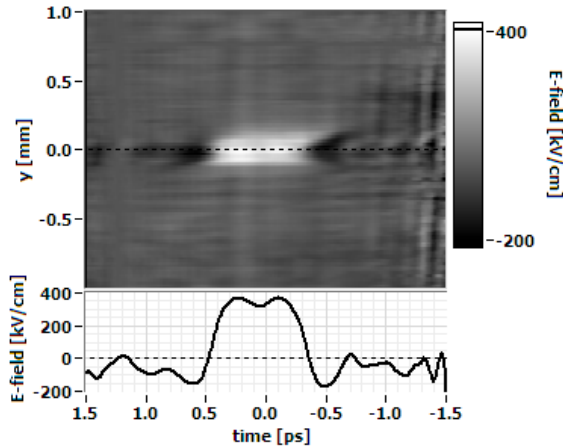


**FIGURE 5.** Space-time cross-section of the THz field envelope measured by FDH and lineout.

## CONCLUSION

THz pulses generated by a LWFA were characterized using four distinct techniques providing measurements of pulse duration, energy, and spatio-temporal electric-field profiles. Goly cell measurements are ideal for quick measurements of pulse energy and mode distributions of large beams, but have low dynamic range and no intensity or field information. The non-sign-resolved EO technique is ideal for measuring energy distributions, especially with low field strengths, while the sign-resolved EO technique is good for spatial field mapping but requires a time-consuming scanning

process to recover temporal information. FDH promises to be an ideal compromise, sacrificing one spatial degree of information in order to allow spatio-temporal field mapping in a single shot. In addition, it is not plagued by a  $\pi/2$  limitation on the measurable phase shift, allowing it to measure field strengths greater than 1 MV/cm. These measurements are consistent with each other to first order and indicate THz pulse energies in the range of 5 – 10  $\mu$ J, peak fields of 200 – 400 kV/cm, and pulse durations of about 0.4 - 1.0 ps. Together these techniques form a comprehensive suite of diagnostics for characterization of the THz pulses.

## ACKNOWLEDGMENTS

This research was supported by grants from DARPA and DOE, under contract No. DE-AC02-05CH11231.

## REFERENCES

1. W. P. Leemans et al., *Phys. Rev. Lett.* **91**, 074802 (2003).
2. C. B. Schroeder, E. Esarey, J. van Tilborg, and W.P. Leemans, *Phys. Rev. E* **69**, 016501 (2004).
3. W.P. Leemans, J. van Tilborg, J. Faure, C.G.R. Geddes, Cs. Tóth, C.B. Schroeder, E. Esarey, G. Fubiani, and G. Dugan *Phys. Plasmas* **11**, 2899 (2004).
4. J. van Tilborg, C. B. Schroeder, C.V. Filip, Cs. Tóth, C.G.R. Geddes, G. Fubiani, R. Huber, R.A. Kaindle, E. Esarey, and W.P. Leemans, *Phys. Rev. Lett.* **96**, 014801 (2006).
5. E. Chiadroni, H. Delsim-Hashemi, L. Fröhlich, and O. Grimm, "Report on the visit at FELIX" (2005).
6. J. van Tilborg, "Coherent terahertz radiation from laser-wakefield-accelerated electron beams", Ph.D. Thesis, Eindhoven Technical University, 2006.
7. A. Yariv, *Quantum Electronics*, 3<sup>rd</sup> Ed., New York: John Wiley & Sons, 1989, p. 305.
8. S. P. Le Blanc, E. W. Gaul, N. H. Matlis, A. Rundquist, and M. C. Downer, *Optics Letters* **25**, 764-766 (2000).
9. N.H. Matlis S. Reed, S. S. Bulanov, V. Chvykov, G. Kalintchenko, T. Matsuoka, P. Rousseau, V. Yanovsky, A. Maksimchuk, S. Kalmykov, G. Shvets, and M. C. Downer, *Nature Physics* **2**, 749 (2006).